JGR Atmospheres

RESEARCH ARTICLE
10.1029/2023JD040497

Propagation Effects of Slanted Narrow Bipolar Events: A Rebounding-Wave Model Study

Dongshuai Li[1,2], Alejandro Luque[2], Farhad Rachidi[3], Marcos Rubinstein[4], Torsten Neubert[1], Yanan Zhu[5], Olivier Chanrion[1], Caitano da Silva[6], and Paul R. Krehbiel[6]

[1]National Space Institute, Technical University of Denmark (DTU Space), Kongens Lyngby, Denmark, [2]Instituto de Astrofísica de Andalucía (IAA), CSIC, Granada, Spain, [3]Electromagnetic Compatibility Laboratory, Swiss Federal Institute of Technology (EPFL), Lausanne, Switzerland, [4]University of Applied Sciences and Arts Western Switzerland, Yverdon-les-Bains, Switzerland, [5]Earth Networks, Germantown, MD, USA, [6]Langmuir Laboratory for Atmospheric Research, New Mexico Institute of Mining and Technology, Socorro, NM, USA

Key Points:

- The propagation effect of slanted Narrow bipolar events (NBEs) at different distance is investigated and compared with the observations
- The inclination of the NBEs could significantly affect the electromagnetic fields in the close distance
- The proposed equations will improve the quality of inferred features of slanted NBEs and can be extended to any discharge shape

Supporting Information:

Supporting Information may be found in the online version of this article.

Correspondence to:

D. Li and A. Luque,
dongshuai@space.dtu.dk;
aluque@iaa.es

Citation:

Li, D., Luque, A., Rachidi, F., Rubinstein, M., Neubert, T., Zhu, Y., et al. (2024). Propagation effects of slanted narrow bipolar events: A rebounding-wave model study. *Journal of Geophysical Research: Atmospheres*, *129*, e2023JD040497. https://doi.org/10.1029/2023JD040497

Received 6 DEC 2023
Accepted 10 JUL 2024

Abstract Narrow bipolar events (NBEs) are impulsive and powerful intracloud discharges. Recent observations indicate that some NBEs exhibit a slanted orientation rather than strictly vertical. This paper investigates the effect of the slanted NBEs using a newly developed rebounding-wave model. The modeling results are validated against the full-wave Finite- Difference Time-Domain method and compared with measurements for both vertical and slanted NBE cases. It is found that the inclination of the NBEs affects both the waveforms and amplitudes of the electrostatic, induction and radiation components of the electric fields at close distances (≤10 km). However, it primarily influences the amplitudes of the fields for distances beyond 50 km, where the radiation component dominates, resulting in changes of ≥30% when the slant angle exceeds 30°. The slanted rebounding-wave model improves the agreement with respect to a purely vertical channel and can be extended to any discharge geometry at arbitrary observation distances.

Plain Language Summary Narrow Bipolar Events (NBEs) are unique intracloud discharges that occur either individually or as the initiation event for lightning flashes inside thunderstorms. Knowing the physical mechanisms of NBEs will help us to better understand how lightning initiates inside thunderstorms. Recent studies indicated that NBEs could exhibit a slanted orientation rather than being strictly vertical. However, the inclination of NBEs has not been considered in previous transmission line models, leading to uncertainty when evaluating their characteristics based on electromagnetic fields. Here, in the light of recent observations, we analyze the propagation effect of the slanted NBEs by using a newly developed slanted rebounding-wave model, and we compare the modeling results with observations. This study contributes to a better understanding of the physical mechanism of NBEs and provides a reference for accurately characterizing NBEs based on their electromagnetic fields.

1. Introduction

In recent years, narrow bipolar events (NBEs) have received significant attention. NBEs are radio-frequency emissions from a special type of intracloud discharge, known as Compact Intracloud Discharges (CIDs), but often in the literature, NBEs are commonly used to denote the discharge itself. NBEs appear either isolated or as the initial event of a lightning flash (Leal & Rakov, 2019; Lyu et al., 2019; T. C. Marshall et al., 2019; Rison et al., 2016; Tilles et al., 2019) with strong radiation in the high and very high frequency (HF/VHF) range (Le Vine, 1980; Smith et al., 1999, 2004), and they are characterized by fast breakdowns (FBs) that appear to be a system of streamer coronas (Attanasio et al., 2019, 2021; Liu et al., 2019; Lyu et al., 2019; Phelps, 1974; Phelps & Griffiths, 1976; Rison et al., 2016; Tilles et al., 2019). However, the exact physical mechanism behind NBEs still remains unclear.

The transmission line (TL) model is widely recognized as the most commonly used approach for inferring the characteristics of NBEs based on their electromagnetic fields. NBEs typically have channel lengths ranging from hundreds of meters to a few kilometers (Smith et al., 1999, 2004). Many studies simplify the NBE channel by assuming it to an infinitely short dipole, sometimes referred to as the "Hertzian dipole" (Eack, 2004; Nag & Rakov, 2010; Smith et al., 1999, 2004) or by considering them as small-scale streamer systems while neglecting streamer geometries (Liu & Dwyer, 2020). Therefore, the TL-based models of NBEs are proposed in the

literature. These models include the classic TL model (Watson & Marshall, 2007), the modified transmission line with exponential increase (MTLEI) model (Watson & Marshall, 2007), the bouncing-wave TL model (Nag & Rakov, 2010), the modified TL with exponential decay (MTLE) model (Karunarathne et al., 2016; Rison et al., 2016) and the modified transmission line-gaussian (MTLG) model (da Silva et al., 2016; R. A. Marshall et al., 2015). Attanasio et al. (2021) argued that, from an electrostatic standpoint, the precursor streamer system can produce a strong electric field enhancement ahead of itself that may trigger a rebounding opposite-polarity event traveling back toward the origin. Recently, Li, Luque, Gordillo-Vázquez et al. (2022) introduced a rebounding-wave model based on the Modified TL with Exponential decay (MTLE) model (Nucci & Rachidi, 1989; Rachidi & Nucci, 1990; Rison et al., 2016), termed "rebounding MTLE model", to represent the subsequent streamer features involved in NBEs (Attanasio et al., 2021; Rison et al., 2016; Tilles et al., 2019). A common feature of all the TL-based models is the assumption that the NBE channel is vertically oriented.

Recent observations indicate that NBEs could be tilted from vertical and exhibit a noticeable spread in azimuthal values (Rison et al., 2016). Karunarathne et al. (2016) estimated the three-dimensional charge moments of 10 NBEs and found that three of them were tilted at angles ranging from 10 to 20° from the vertical. R. A. Marshall et al. (2015) suggested that slanted NBEs play a role in the illumination of the lower ionosphere known as "elve doublets". Particularly, these authors suggested that if the NBE source current is inclined toward the observer, the second elve in the doublet can be brighter than the first. However, the impact of channel inclination on the propagation effects of NBEs at different distances remains unknown. Here, following previous studies on the effect of the inclination and tortuosity of lightning return stroke channels (Abouzeid et al., 2015; Le Vine & Meneghini, 1978a, 1978b), we propose an extension of the rebounding wave model of Li, Luque, Gordillo-Vázquez et al. (2022) for NBEs. The so-called slanted rebounding wave model is firstly validated against a full-wave three-dimensional Finite-Difference Time-Domain (FDTD) method and then through comparisons with observations reported in the literature.

2. Slanted Rebounding Wave Model

The slanted TL model was proposed by Abouzeid et al. (2015) to analyze the effect of lightning return stroke channel tortuosity and branching, and by Andreotti et al. (2012) to examine the lightning electric fields and the voltages induced on overhead conductors. In this study, we extend their equations to investigate the inclination of the NBE channel. NBE is considered as a system of streamer coronas represented by the a rebounding-wave model based on the Modified TL with Exponential decay (MTLE) (Nucci & Rachidi, 1989; Rachidi & Nucci, 1990; Rison et al., 2016), termed "rebounding MTLE model" (Li, Luque, Gordillo-Vázquez et al., 2022).

As illustrated in Figure 1, the positive streamer coronas propagate downwards from an altitude H_2 to an altitude H_1 with a channel length L (for a slanted channel $H_1 = H_2 - r\cos\theta$), followed by upward negative streamer corona discharges that propagate back along the same path. I_d is the downward current (red color) and I_u is the rebounding-wave current (blue color). According to the rebounding MTLE model (Li, Luque, Gordillo-Vázquez et al., 2022), the total current $I(r, t)$ is the sum of the downward current $I_d(r, t)$ and the upward rebounding current $I_u(r, t)$. Both currents are assumed to experience an exponential decay along the same propagation channel with attenuation rates of λ_d and λ_u, respectively. The total current and the downward and upward rebounding currents are given by

$$\begin{aligned} I(r,t) &= I_d(r,t) + I_u(r,t), \\ I_d(r,t) &= I(t-(L-r)/v_d)\, e^{-(L-r)/\lambda_d}, \\ I_u(r,t) &= I(t-L/v_d - r/v_u)\, e^{-L/\lambda_d} e^{-r/\lambda_u}, \end{aligned} \tag{1}$$

where v_d and v_u are the downward and upward propagation velocities. e^{-L/λ_d} ensures the continuity between the downward and the upward-propagating currents.

The equations for the electromagnetic field created by a slanted dipole were described by Abouzeid et al. (2015); Andreotti et al. (2012). Adapting them to geometry represented in Figure 1, in free space, the vertical electric field E_z at the observation point $P(x_p, y_p, z_p)$, where $x_p = \rho\cos(\phi_p)$ and $y_p = \rho\sin(\phi_p)$, due to a short inclined dipole dr carrying the current $I(r, t)$ located at a height $(H_2 - r\cos\theta)$ is given as:.

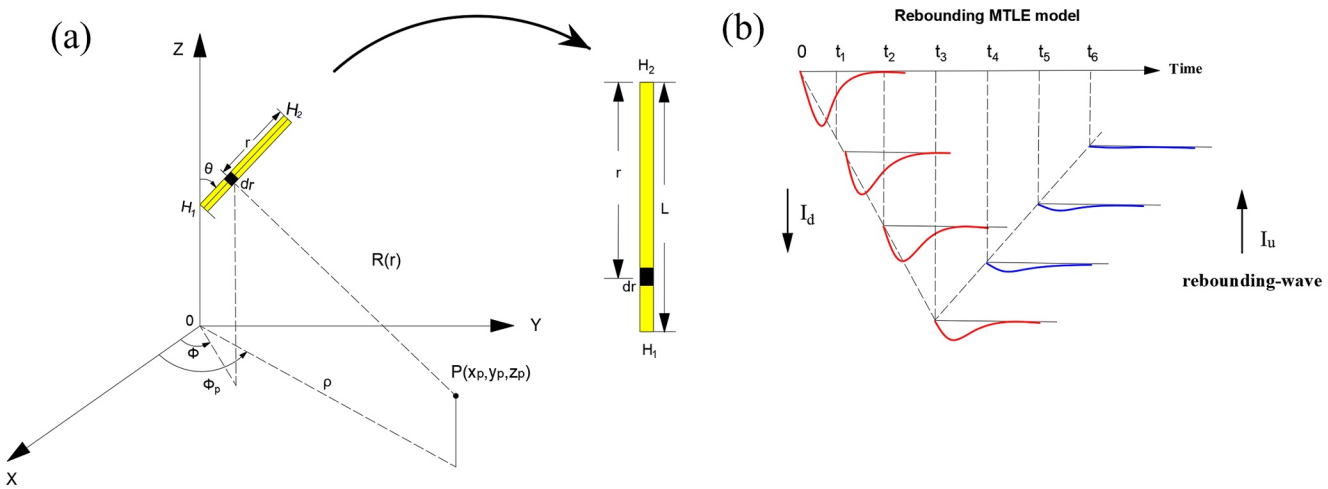

Figure 1. Geometry of the inclined NBE channel with a current that propagates following the rebounding MTLE model. (a) We model the NBE channel as a series of small straight segments at a radial distance of r and a polar angle θ with respect to the Z axis. The azimuth angle ϕ is defined by the angle between the X axis and the projection of the segment in the XY plane. The observation point $P(x_p, y_p, z_p)$ is at an altitude z_p above the ground surface and at a plane distance ρ from the source, thus $x_p = \rho \cos(\phi_p)$, $y_p = \rho \sin(\phi_p)$, where ϕ_p is the azimuth angle of the observation point P. (b) In the rebounding MTLE model, the NBE channel is considered as a system of positive streamer coronas that propagate downward from an altitude H_2 to H_1 with a channel length L, followed by upward negative streamer corona discharges that propagate back along the same path. Here, I_d is the downward current (red color) and I_u is the rebounding-wave current (blue color).

$$
\begin{aligned}
dE_{zc} = \frac{dr}{4\pi\varepsilon_0}
&\left(
\begin{aligned}
&\left(
\begin{aligned}
&\frac{3(z_p-(H_2-r\cos\theta))\,(x_p-r\sin\theta\cos\phi)}{R^5(r)}\sin\theta\cos\phi\\
&+\frac{3(z_p-(H_2-r\cos\theta))\,(y_p-r\sin\theta\sin\phi)}{R^5(r)}\sin\theta\sin\phi\\
&+\frac{3(z_p-(H_2-r\cos\theta))^2-R^2(r)}{R^5(r)}\cos\theta
\end{aligned}
\right)\int_0^t I(r,t)d\tau\\
&\left(
\begin{aligned}
&\frac{3(z_p-(H_2-r\cos\theta))\,(x_p-r\sin\theta\cos\phi)}{cR^4(r)}\sin\theta\cos\phi\\
&+\frac{3(z_p-(H_2-r\cos\theta))\,(y_p-r\sin\theta\sin\phi)}{cR^4(r)}\sin\theta\sin\phi\\
&+\frac{3(z_p-(H_2-r\cos\theta))^2-R^2(r)}{cR^4(r)}\cos\theta
\end{aligned}
\right)I(r,t)\\
&\left(
\begin{aligned}
&\frac{(z_p-(H_2-r\cos\theta))\,(x_p-r\sin\theta\cos\phi)}{c^2R^3(r)}\sin\theta\cos\phi\\
&+\frac{(z_p-(H_2-r\cos\theta))\,(y_p-r\sin\theta\sin\phi)}{c^2R^3(r)}\sin\theta\sin\phi\\
&+\frac{(z_p-(H_2-r\cos\theta))^2-R^2(r)}{c^2R^3(r)}\cos\theta
\end{aligned}
\right)\frac{\partial I(r,t)}{\partial t}
\end{aligned}
\right),
\end{aligned}
\tag{2}
$$

where,

$$R(r) = \sqrt{(x_p - r\sin\theta\cos\phi)^2 + \left(y_p - r\sin\theta\sin\phi\right)^2 + (z_p - (H_2 - r\cos\theta))^2}. \tag{3}$$

Individual terms on the right hand side of Equation 2 containing the factors are the electrostatic, induction and radiation components. If we assume the ground as a perfectly conducting plane, its effect can be taken into account using image theory, yielding

$$dE_{zm} = -\frac{dr}{4\pi\varepsilon_0}\left(\begin{array}{l}\left(\begin{array}{l}\dfrac{3(z_p + (H_2 - r\cos\theta))(x_p - r\sin\theta\cos\phi)}{R_0^5(r)}\sin\theta\cos\phi \\ +\dfrac{3(z_p + (H_2 - r\cos\theta))\left(y_p - r\sin\theta\sin\phi\right)}{R_0^5(r)}\sin\theta\sin\phi \\ -\dfrac{3(z_p + (H_2 - r\cos\theta))^2 - R_0^2(r)}{R_0^5(r)}\cos\theta\end{array}\right)\int_0^t I(r,t)d\tau \\ \left(\begin{array}{l}\dfrac{3(z_p + (H_2 - r\cos\theta))(x_p - r\sin\theta\cos\phi)}{cR_0^4(r)}\sin\theta\cos\phi \\ +\dfrac{3(z_p + (H_2 - r\cos\theta))\left(y_p - r\sin\theta\sin\phi\right)}{cR_0^4(r)}\sin\theta\sin\phi \\ -\dfrac{3(z_p + (H_2 - r\cos\theta))^2 - R_0^2(r)}{cR_0^4(r)}\cos\theta\end{array}\right)I(r,t) \\ \left(\begin{array}{l}\dfrac{(z_p + (H_2 - r\cos\theta))(x_p - r\sin\theta\cos\phi)}{c^2R_0^3(r)}\sin\theta\cos\phi \\ +\dfrac{(z_p + (H_2 - r\cos\theta))\left(y_p - r\sin\theta\sin\phi\right)}{c^2R_0^3(r)}\sin\theta\sin\phi \\ -\dfrac{(z_p + (H_2 - r\cos\theta))^2 - R_0^2(r)}{c^2R_0^3(r)}\cos\theta\end{array}\right)\dfrac{\partial I(r,t)}{\partial t}\end{array}\right), \tag{4}$$

where,

$$R_0(r) = \sqrt{(x_p - r\sin\theta\cos\phi)^2 + \left(y_p - r\sin\theta\sin\phi\right)^2 + (z_p + (H_2 - r\cos\theta))^2}. \tag{5}$$

For an observer P located on the ground surface, the height of the observation point z_p is equal to zero in all the equations above, implying $R = R_0$. The total vertical electric field E_z for the whole inclined channel can be obtained by integrating the dipole field dE_{zc} and its image dE_{zm} over the entire channel. Note that both the dipole field dE_{zc} and its image dE_{zm} include the slanted feature of the sources, and they reduce to the case of a vertical

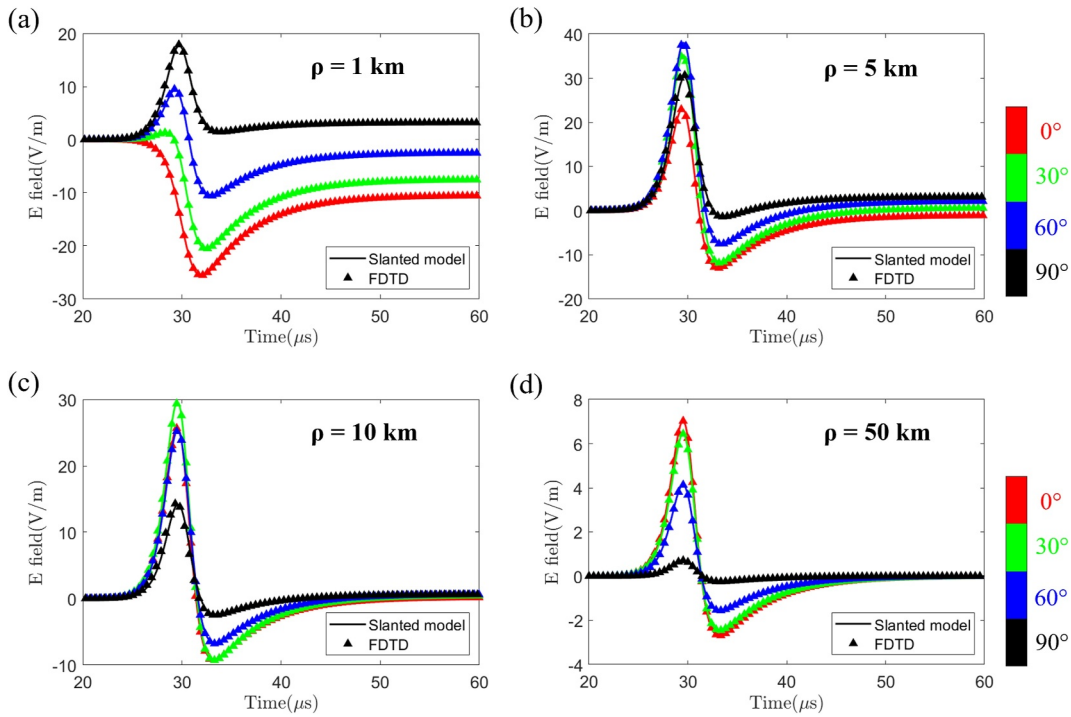

Figure 2. Comparison between the slanted rebounding wave model and FDTD method by considering the slanted dipole with different θ angles with respect to the z-axis and the azimuthal angle $\phi = 0°$ at a distance of 1, 5, 10, and 50 km.

channel when the polar angle $\theta = 0$ (Thottappillil & Rakov, 2001; Uman et al., 1975). Moreover, the equations are not limited to straight channel but also can be applied to any arbitrarily tortuous discharge channel by approximating it as a series of small straight segments.

Although not mentioned in the study of Abouzeid et al. (2015), the so-called discontinuity term (Thottappillil et al., 1998; Thottappillil & Rakov, 2001),"turn-on" term (Uman & McLain, 1970a, 1970b) or F factor (Rubinstein & Uman, 1990; Shao et al., 2004, 2005; Thottappillil & Rakov, 2001, 2005) should be considered if there is a current discontinuity at the propagation wave front. The equations for the discontinuity term are given in Text S1 in Supporting Information S1.

3. Validation of the Slanted Rebounding Wave Model

To validate the proposed slanted TL equations for NBEs, we compare its prediction against a full-wave three-dimensional FDTD model (Li et al., 2016, 2017). In the simulation, the NBE source is assumed to be a dipole at an altitude $H = 5$ km above a perfectly conducting ground with different polar angle θ of 0°, 30°, 60° and 90°. The current waveform is given by double-exponential expression with $I(t) = I_0(e^{\alpha t}/(1 + e^{(\alpha+\beta)t})$, where the rise time constant is $\alpha = 1/\tau_1$ and the fall time constant is $\beta = 1/\tau_2$ (Rison et al., 2016). The values of τ_1 and τ_2 are 1 and 5 μs, respectively. The peak current is normalized to $I_{peak} = -100$ kA by setting $I_0 = I_{peak}\left(1 + \frac{\alpha}{\beta}\right)\left(\frac{\alpha}{\beta}\right)^{\left(\frac{-\alpha}{\alpha+\beta}\right)}$. The observation point P is located at a distance ρ with the azimuthal angle $\phi_p = 0°$.

The comparison between the slanted rebounding wave model and the FDTD method for both vertical and slanted dipoles is given in Figure 2. The results calculated by the presented equations match perfectly with the FDTD results for both vertical and slanted sources. For horizontal dipole with $\theta = 90°$, the electric field first increases within a distance of 5 km and then decreases as the observer moves away from the source and becomes negligible beyond a distance of about 50 km.

The results from the FDTD simulation are further shown in Figures S1 and S2 in Supporting Information S1. Figures S1 and S2 in Supporting Information S1 show the cross sections in XOZ plane, XOY plane and YOZ

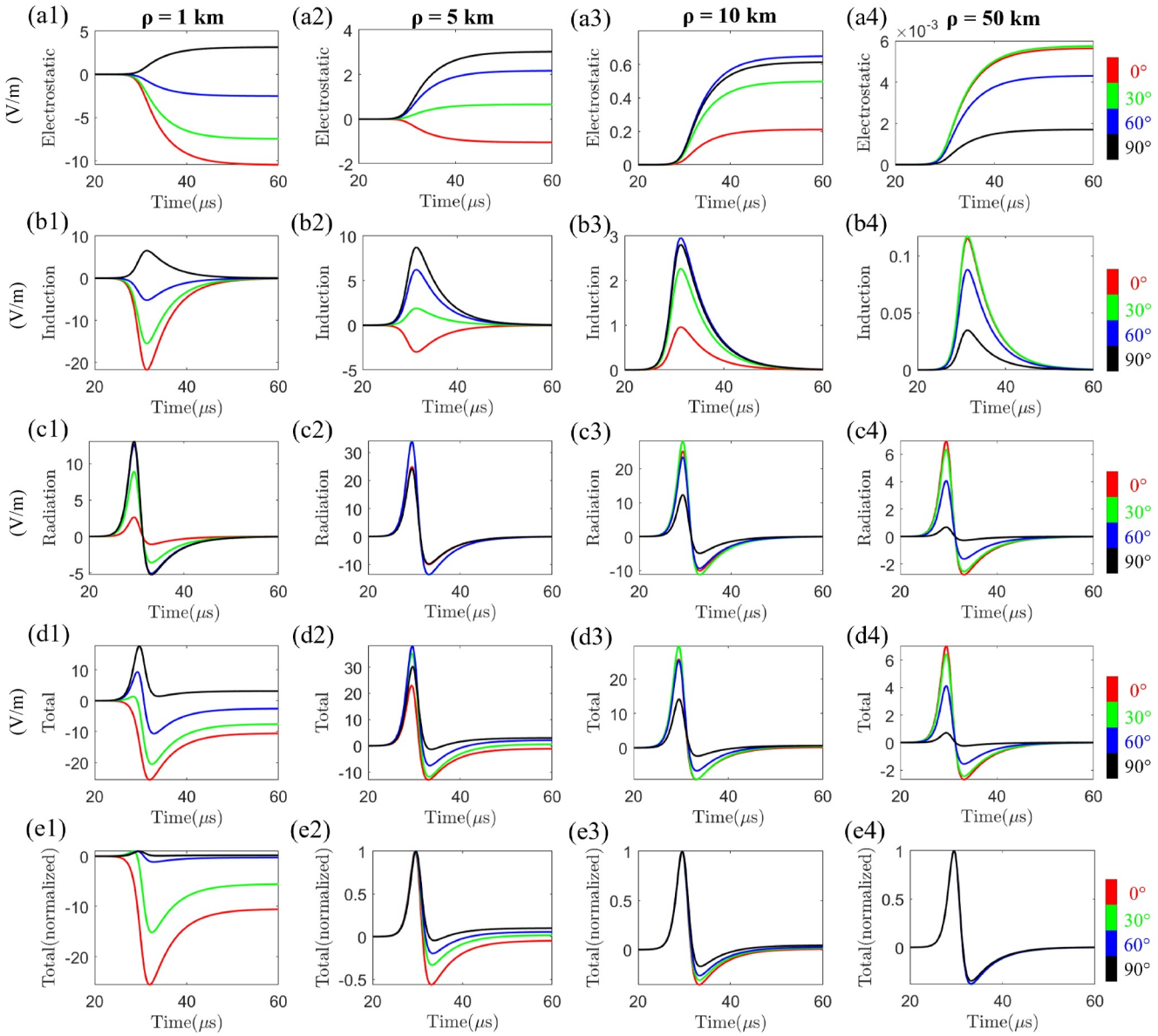

Figure 3. Electrostatic (a1–a4), Induction (b1–b4), and Radiation (c1–c4) components of the total electric fields (d1–d4) and the normalized total electric fields (e1–e4) for the slanted dipole with different θ angles with respect to Z axis and the azimuthal angle $\phi = 0°$ at a distance of 1, 5, 10, and 50 km.

plane of the FDTD simulation for the vertical electric fields of the slanted dipole with $\theta = 0°$, 30°, 60° and 90°. For a vertical dipole with $\theta = 0°$, the electric field exhibits azimuthal symmetry, but it is more complicated for the slanted cases showing different features depending on the observed directions and distances. The difference between positive and negative values of the x coordinate increases as the change of the polar angles from 0° to 60°. In the case of a horizontal dipole, the pattern of the vertical electric field in the YOZ plane reverses between positive and negative values of the x coordinate (see Figures S2g and S2h in Supporting Information S1).

Figure 3 illustrates the electrostatic, induction and radiation components for both vertical and slanted dipoles at different distances. The inclination of the source at closer distances (≤10 km) causes a significant effect on the electrostatic and induction components of the electric fields. Both the waveshape and the amplitude of the electric field are influenced by the inclination of the source (see Figures 3d1, 3d2, and 3d3)). In our case, the reversal distance (Nag & Rakov, 2010), where the electrostatic and induction components of the field reverse their

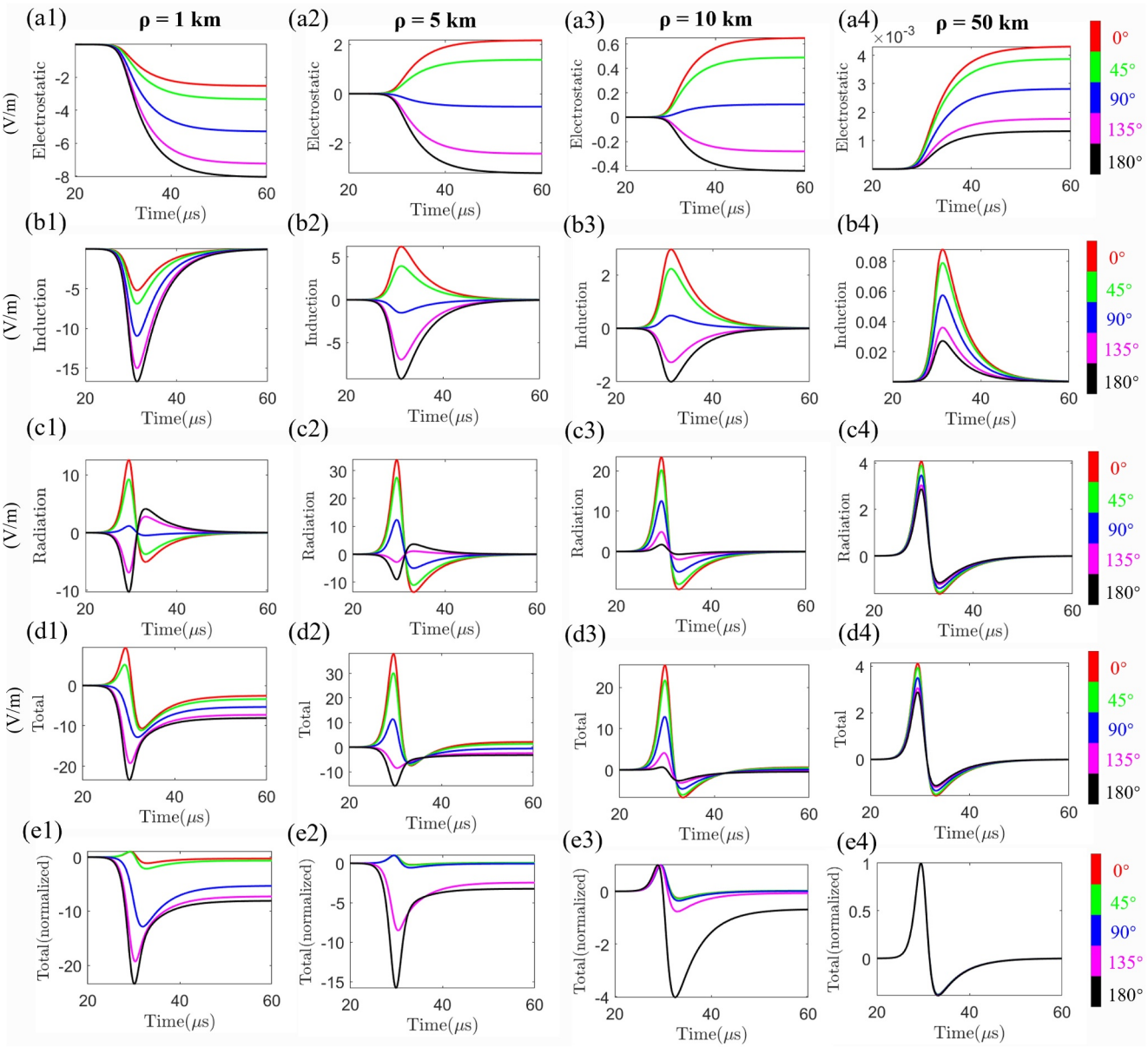

Figure 4. Electrostatic (a1–a4), Induction (b1–b4), and Radiation (c1–c4) components of the total electric fields (d1–d4) and the normalized total electric fields (e1–e4) for the slanted dipole with the polar angle $\theta = 60°$ and different ϕ angles at a distance of 1, 5, 10, and 50 km.

polarity, varies as a function of the slanted dipole angle. As shown in Figures 3d2, 3d3, 3e2, and 3e3), the tail part of the waveform becomes higher due to the increase of the electrostatic fields caused by the slant angle. For distances beyond 50 km, the electric field is dominated by the radiation component, and the inclination only affects the amplitudes (see Figures 3d4 and 3e4)). It is interesting to note that the effect of slant angles bigger than 30° can cause changes in field amplitude exceeding 30% even at distances as large as 50 km (see Figure 3d4)).

Figure 4 shows the electrostatic, induction and radiation components for a slanted dipole with $\theta = 60°$ and $\phi = 0°$, 45°, 90°, 135° and 180°. The amplitude and polarity of the electrostatic, induction, and radiation components can be influenced by changes in azimuthal angles at distances shorter than 10 km. When the distance exceeds 50 km, the peak of the vertical electric field decreases by approximately 10% as the azimuthal angle changes from 0° to 180° (see Figure 4d4).

4. Comparison With the Observations in the Literature

4.1. The Electrical Discharges Following NBEs

Recent studies reported that the electric fields of NBEs at distances below 10 km include two parts: a main bipolar pulse characteristic of NBE and a slow electrostatic change lasting from tens of microseconds to a few milliseconds (Karunarathne et al., 2016; T. C. Marshall et al., 2014). The slow electrostatic change following NBEs seems to be related to the attempted electrical activities that never developed into a full lightning flash (Karunarathne et al., 2016). This fact is also supported by the multi-pulse corona discharges observed by the Atmosphere-Space Interactions Monitor (ASIM) onboard International Space Station (ISS) (Li, Luque, Gordillo-Vazquez et al., 2023; Li, Luque, Lehtinen, et al., 2022). In their study, Li, Luque, Lehtinen, et al. (2022) found that, for the multi-pulse corona discharges, the first optical pulse coincides with a strong radio signal in the form of a NBE but subsequent optical pulses, delayed by some milliseconds, are related to horizontally oriented streamer-like electrical discharges which do not trigger full-fledged lightning. More recently, Chen et al. (2024) found that there were small but well-defined secondary pulses following the main pulse (including its opposite polarity overshoot) of the over-water CID clusters over time intervals up to 80 μs or so. However, it remains unclear whether these electrical discharges following NBEs are part of the NBEs produced by the remaining streamer corona activities (Li, Luque, Gordillo-Vázquez et al., 2022; Rison et al., 2016) or if they are a weakly conducting resonant cavity in the wake caused by the NBE's streamers (Senay et al., 2023) or if they are independent electrical discharges, similar to the Initial E-Change (IEC) that occurs before the first initial breakdown pulses of a lightning flash (T. C. Marshall et al., 2014, 2019; Kostinskiy et al., 2020).

In our study, we consider these electrical discharges as an extra long decay current I_{extra} along with the main NBE current, despite lacking knowledge about their physical mechanism. The current is represented using the double-exponential expressions (Rison et al., 2016),

$$I(t) = I_{NBE}(t) + I_{extra}(t) = I_0 \frac{e^{\alpha t}}{1 + e^{(\alpha+\beta)t}} + \eta I_0 \frac{e^{\alpha t}}{1 + e^{(\alpha+\gamma)t}}, \tag{6}$$

where the rise time constant for the original streamer current $\alpha = 1/\tau_1$ and the fall time constant for the original streamer current $\beta = 1/\tau_2$. For the extra current $\gamma = 1/\tau_3$. $0 \le \eta \le 1$ is the fraction of the extra current $I_{extra}(t)$ compared to the primary NBE current $I_{NBE}(t)$. The peak value of I_{NBE} is normalized to I_{peak} by setting $I_0 = I_{peak}\left(1 + \frac{\alpha}{\beta}\right)\left(\frac{\alpha}{\beta}\right)^{\left(\frac{-\alpha}{\alpha+\beta}\right)}$.

4.2. Comparison With the Observations Reported by Rison et al. (2016)

In this section, we compare the simulated results obtained by the slanted rebounding wave model with the electric fields measured by a fast antenna (FA) for the vertical and slanted cases reported by Rison et al. (2016). According to interferometer (INTF) observations, the NBEs consisted of a downward Fast Positive Breakdown (FPB) followed immediately by an upward Fast Negative Breakdown (FNB) that propagated back in the opposite direction along the previous path. In the simulation, we model the FB of the NBE as a system of positive streamers that propagate downwards over a distance L, then upwards back along the previous path as predicted by the rebounding MTLE model (Li, Luque, Gordillo-Vázquez et al., 2022). The same double-exponential current is adopted for the comparison with the results of Rison et al. (2016).

According to Equation 1, the total current $I(r, t)$ is the sum of the downward current $I_d(r, t)$ and the upward rebounding current $I_u(r, t)$, where $v_d = L/t_d$ and $v_u = L/t_u$ are the downward and upward velocities related to the inferred downward and upward propagation times t_d and t_u obtained by fitting the INTF traces for both NBE1 and NBE3 with the best fit lines shown in Li, Luque, Gordillo-Vázquez et al. (2022) (see Figure 2 there).

As mentioned by Rison et al. (2016), the NBE1 discharge occurred at constant azimuth consistent with the positive breakdown being vertically downward (see Figure 7 in the Supplementary Material of Rison et al. (2016)). On the other hand, NBE3 showed substantial azimuthal spread with nonnegligible tilt from vertical (see Figure 9 in the Supplementary Material of Rison et al. (2016)). Firstly, we assume the channel to be vertical ($\theta = 0°$) for both NBE1 and NBE3. Note that the results by assuming both NBE1 and NBE3 to be vertical are discussed in Li, Luque, Gordillo-Vázquez et al. (2022). Here we also present the results in Figure 5, which are obtained using the least-squares curve fitting method with initial values listed in Table 1. We checked the robustness of the best-fit parameters (see Table 2) by performing the least-squares fitting with somewhat different initial guesses and confirming that it converges on the same final values. The estimated charge moment change Q_{mom} for the vertical NBE1 and vertical NBE3 are -215 C· m and -116 C· m, respectively. It is found that the simulated results for NBE1 agree well with the observations. However, this is not the case for the slanted case of NBE3, for which significant deviations can be observed, especially in the tail part of the waveform.

In order to investigate the effect of the inclination of NBE sources on the fields, we introduce an additional free parameter, the polar angle θ, to represent the effect of inclination. To simplify the geometry, we assume that the plane containing the NBE channel is perpendicular to the transfer vector from the INTF observations' geometry to the geometry used in Figure 1 (see Text S2 and Figure S3 in Supporting Information S1). The azimuth angle for the source $\phi = 249°$ and for the observation point P, $\phi_p = 160°$, are estimated based on the transformation. The simulated result for the slanted NBE3 is presented in Figure 5c with the inferred features shown in Table 2. By considering the simulation-estimated polar angle of $\theta = 15°$, the simulated waveform for NBE3 reasonably agrees with the measurement, corresponding to a charge moment change of -357 C· m, which is three times larger than the vertical case. However, the observed flattening tail part of NBE3 still could not be matched well. This suggests that NBE3 might involve more complicated processes than just being slanted.

As mentioned earlier, the electrostatic offset of NBE3 could be produced by the remaining streamer activities following NBEs (Rison et al., 2016). To address this, we introduce an additional long decay current, I_{extra}, derived from the presence of the remaining streamer corona activities of NBE3 that last for a few microseconds (see the subsequent signals at 20–50 μs of Figure 2b in Rison et al. (2016)). For comparison, the results for the vertical NBE3 with an extra long decay current I_{extra} are given in Figure 5d with the estimated charge moment change $Q_{\mathrm{mom}} = -201$ C· m. It is noted that the tail part of the electric field improves by adding the extra current, but the head part drifts away from the measurement. The results in Figure 5e show that by considering the extra long decay current I_{extra} and the simulation-estimated angle $\theta = 15°$ with respect to the z-axis, the tail parts of the electrostatic and induction components for NBE3 have been reduced, while the head part of radiation component has been increased, resulting in a better agreement with the observation. In this case, the estimated charge moment change Q_{mom} of the NBE3 is -219 C· m, which is similar to that of vertical NBE1. Both the polar angle and the extra-long decay current could play crucial roles in shaping different segments of the electric fields of NBEs. It is suggested that adding the decay current helps the tail of the electric field, while considering the polar angles improves the head portion.

Figure 6 further shows the current distribution along the channel based on the rebounding MTLE model for the vertical NBE1, the vertical NBE3, the slanted NBE3, the vertical and slanted NBE3 with the extra current I_{extra}. We see that, among all cases, considering the inclination of the channel and the extra long decay current I_{extra} results in the best agreement with the INTF traces. This is consistent with the observations showing substantial azimuthal spread indicating a tilted channel.

In addition, we compared the simulated results at 497 km using the rebounding MTLE model for NBE1 and NBE3 discharges with the observations from Rison et al. (2016) in Figure S4 in Supporting Information S1. It is noted that our modeling results slightly differ from those in Supplementary Figure 14 of Rison et al. (2016). There is no discontinuity at the far end of the channel, as discussed in Pervez et al. (2024); Li, Luque, Gordillo-Vázquez et al. (2022), since the upward current pulse of the NBE is attenuated to a negligible value before it reaches the upper boundary in the rebounding MTLE model. The discrepancies in

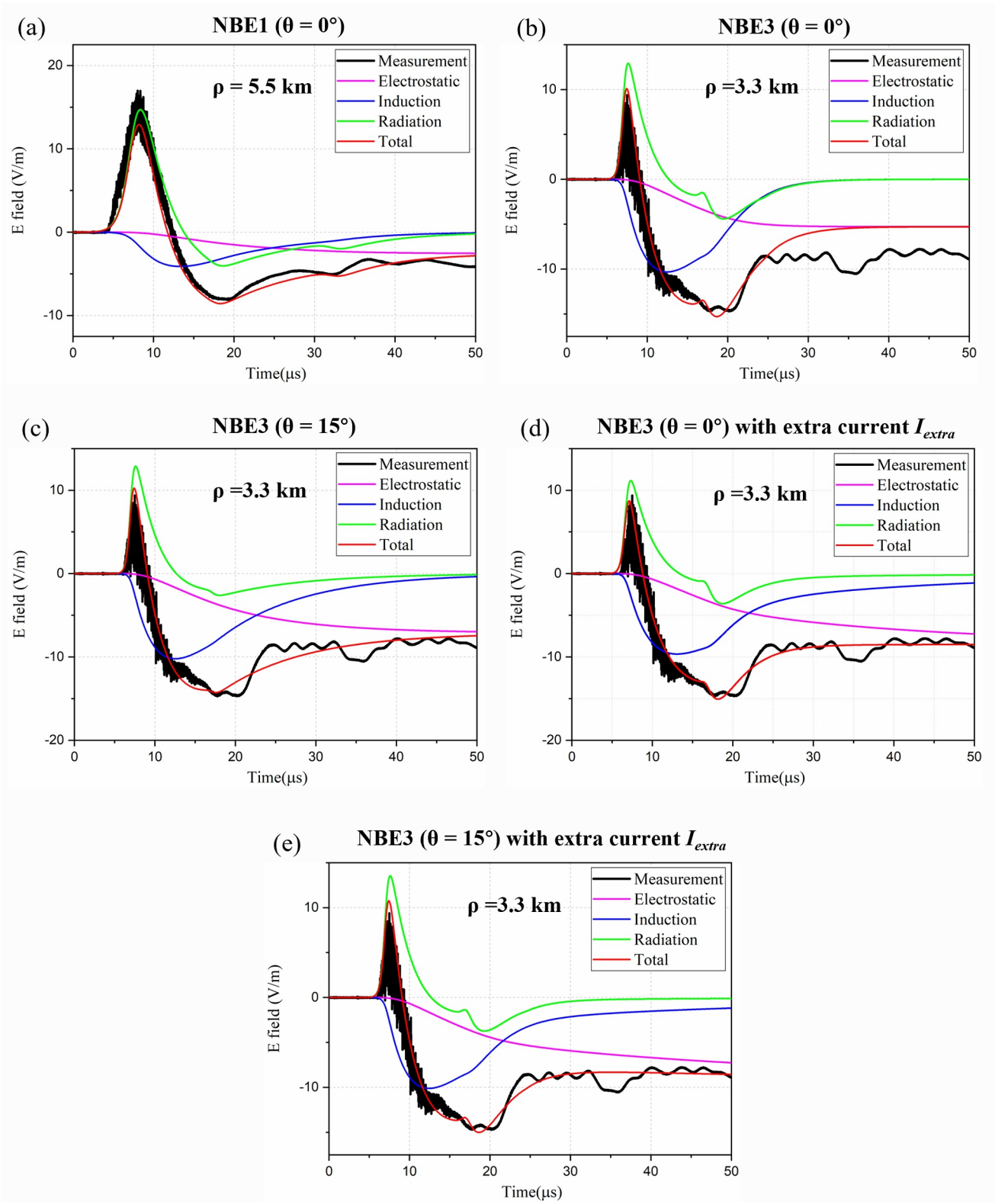

Figure 5. Comparison between the observations from Rison et al. (2016) and simulation results by assuming the vertical channel for NBE1(a) and NBE3(b) and the slanted channel for NBE3 (c) and the vertical (d) and slanted (e) channel for NBE3 with the extra current I_{extra}. The electrostatic, induction and radiation components of the total electric fields are also given in the figure.

Table 1
The Initial Values of the Least Squares Fit for the Vertical NBE1, the Vertical NBE3, the Slanted NBE3, the Vertical and Slanted NBE3 With the Extra Current I_{extra}, the Vertical NBE#174, the Vertical NBE#92, and the Slanted NBE#92

		Initial values							
ID	Inclination	Polar angle θ	I_{peak} (kA)	τ_1 (μs)	τ_2 (μs)	I_{peak}^{extra} (kA)	τ_3 (μs)	λ_d (m)	λ_u (m)
NBE1	Vertical	–	−10.0	0.1	1.0	–	–	500.0	500.0
NBE3	Vertical	–	−10.0	0.1	1.0	–	–	500.0	500.0
	Slanted	10°	−10.0	0.1	1.0	–	–	500.0	500.0
	Vertical	–	−10.0	0.1	1.0	−1.0	10.0	500.0	500.0
	Slanted	10°	−10.0	0.1	1.0	−1.0	10.0	500.0	500.0

		Initial values							
ID	Inclination	Polar angle θ	I_{peak} (kA)	τ_1 (μs)	τ_2 (μs)	I_{peak}^{extra} (kA)	τ_3 (μs)	λ_d (m)	λ_u (m)
NBE#174	Vertical	–	−100.0	1.0	10.0	−10.0	10.0	500.0	500.0
NBE#92	Vertical	–	−100.0	1.0	10.0	−10.0	10.0	500.0	500.0
	Slanted	10°	−100.0	1.0	10.0	−10.0	10.0	500.0	500.0

the results due to the fact that while the results from Rison et al. (2016) account for propagation effects over a finitely conducting earth, our modeling assumes the ground to be a perfectly conducting earth with the boundary condition that the tangential components of the electric field (E_x and E_y) are zero at the surface. The fields are modeled by replacing the ground plane with an image channel. This could lead to discrepancies in the results, especially considering the presence of a large number of high-frequency components in NBEs. As highlighted by Li et al. (2020), finite ground conductivity can notably impact the early time response of the electric fields by attenuating its peak and slowing down its rise time when the observational distances are above 100 km.

Table 2
The Inferred Features of the Fast Breakdowns Corresponding to the Vertical NBE1, the Vertical NBE3, the Slanted NBE3, the Vertical and Slanted NBE3 With the Extra Current I_{extra}, the Vertical NBE#174, the Vertical NBE#92, and the Slanted NBE#92

			Simulation-determined parameters								INTF-determined parameters				
ID	Inclination	Polar angle θ	I_{peak} (kA)	τ_1 (μs)	τ_2 (μs)	I_{peak}^{extra} (kA)	τ_3 (μs)	λ_d (m)	λ_u (m)	Q_{mom} ($C \cdot m$)	P (km)	H_2 (km)	L (m)	t_d[a] (μs)	t_u[a] (μs)
NBE1	Vertical	0°	−30.5	0.8	7.0	–	–	374.9	857.6	−215	5.5	6.7	720	12	13
NBE3	Vertical	0°	−61.7	0.3	3.4	–	–	378.7	113.7	−116	3.3	6.6	412	11	6
	Slanted	15°	−75.0	0.3	10.4	–	–	136.6	22.1	−357	3.3	6.6	412	11	6
	Vertical	0°	−43.9	0.3	3.3	−10.5	27.3	342.5	71.3	−201	3.3	6.6	412	11	6
	Slanted	15°	−56.6	0.3	3.2	−7.4	39.7	305.4	98.3	−219	3.3	6.6	412	11	6

			Simulation-determined parameters								Other parameters		
ID	Inclination	Polar angle θ	I_{peak} (kA)	τ_1 (μs)	τ_2 (μs)	I_{peak}^{extra} (kA)	τ_3 (μs)	λ_d (m)	λ_u (m)	Q_{mom} ($C \cdot m$)	H_2 (km)	L[b] (m)	ν[b] (m/s)
NBE#174	Vertical	0°	−426.5	2.0	1.2	−34.9	78.1	257.3	125.8	−4,775	13	1,000	2.6×10^7
NBE#92	Vertical	0°	−200.6	1.0	31.4	−41.0	196.0	96.2	10^5	−4,519	13.3	300	5×10^7
	Slanted	13°	−345.2	0.9	32.6	−28.9	410.1	66.8	10^5	−6,958	13.3	300	5×10^7

[a]The downward and upward propagation time t_d and t_u are determined by fitting the INTF traces for both NBE1 and NBE3 in Rison et al. (2016). [b]The channel length L and the propagation velocity ν are obtained from Karunarathne et al. (2016); Rison et al. (2016).

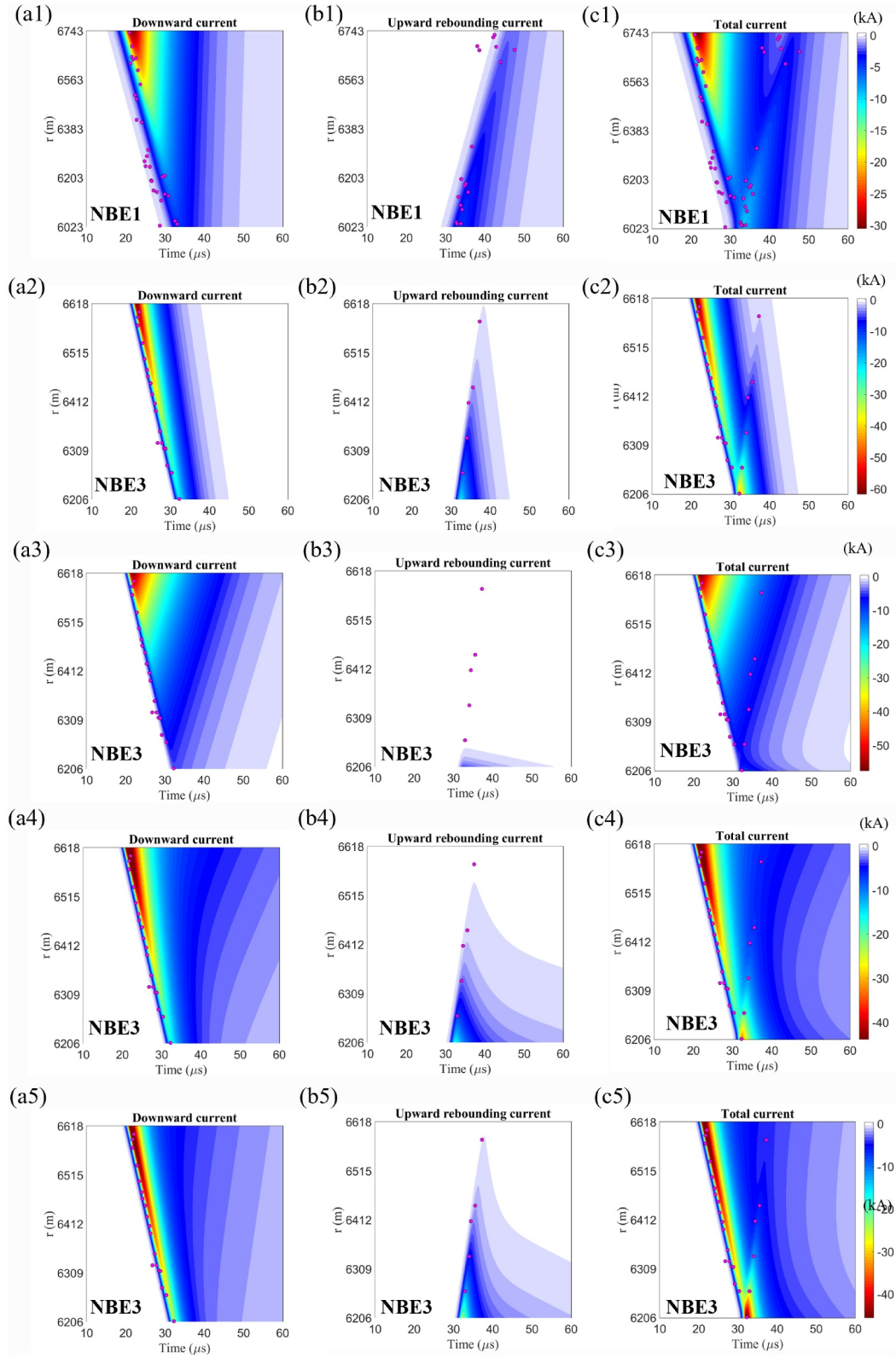

Figure 6. The downward, upward and total current distribution based on the rebounding MTLE model for the vertical NBE1 (a1, b1, c1), the vertical NBE3 (a2, b2, c2), the slanted NBE3 (a3, b3, c3), the vertical NBE3 with the extra current I_{extra} (a4, b4, c4) and the slanted NBE3 with the extra current I_{extra} (a5, b5, c5). The INTF data corresponding to the source time are marked by the pink dots.

4.3. Comparison With the Observations Reported by Karunarathne et al. (2016)

In this section, we compare the simulated results obtained by the slanted rebounding wave model with the electric fields measured by a FA array for the vertical and slanted cases reported by Karunarathne et al. (2016). In their study, Karunarathne et al. (2016) estimated three-dimensional charge moments of 10 NBEs based on a dipole model and found that seven NBEs were essentially vertically oriented, while three NBEs were tilted at angles ranging from 10 to 20° from the vertical. To further investigate the effect of the inclination in the NBE channel, we have chosen two cases: (a) NBE#174 corresponding to a vertical channel, and (b) NBE#92 corresponding to a tilted channel.

Similar to the previous simulations, we consider the FB of NBEs as a system of positive streamers that propagate downwards along a distance L, then upwards back along the previous path, following the rebounding MTLE model (Li, Luque, Gordillo-Vázquez et al., 2022). Since the FBs for both NBE#174 and NBE#92 are followed by slow electrostatic changes, in the simulation, we add the extra long decay current I_{extra} to address the effect of these slow electrostatic changes according to Equation 6.

As shown in Figure 7, for the vertical case NBE#174, with a polar angle $\theta = 0°$, the simulated results considering the extra long decay current I_{extra} agree well with the electric fields measured by different fast antennas located at distances from 9 to 70 km. To compare our modeling results with those of Karunarathne et al. (2016), we assumed a channel length of 1,000 m and a propagation velocity of $\nu = 2.6 \times 10^7$ m/s, both taken form the literature (Karunarathne et al., 2016; Rison et al., 2016). The best-fit parameters are obtained from the least-squares curve fitting by considering the initial values listed in Table 1, which are consistent with those reported by Karunarathne et al. (2016) and shown in Table 2. It is worth noting that although Karunarathne et al. (2016) modeled NBE#174 in their study, they were unable to accurately reproduce the slow electrostatic changes at close stations since they assumed a current for the slow electrostatic change that linearly decreases with time. However, in our case, the observed electrostatic change can be explained by introducing an extra current I_{extra} that follows a double-exponential expression, which suggests that the current of the electrostatic change may actually decrease exponentially, rather than linearly.

The results illustrated in Figures 8a, 8c, 8e, and 8g indicate that by assuming a vertical channel for the slanted case of NBE#92, the simulation does not agree well with the tail part of the observations at close distances, but shows a reasonable agreement beyond a distance of about 10 km. As previously mentioned, this is likely due to the inclination of the NBE sources, as supported by the results shown in Figures 8b, 8d, 8f, and 8h. From Figure 8, we see that when the simulation-estimated angle $\theta = 13°$ with respect to the Z axis is taken into account, the modeling of the tail part corresponding to the electrostatic component improves, resulting in a better agreement with both close and far observations.

The current distribution based on the rebounding MTLE model for the vertical NBE#174, the vertical NBE#92 and the slanted NBE#92 are given in Figure 9 with the detailed inferred parameters given in Table 2. The model-estimated charge moment Q_{mom} for NBE#92 changed from −4,519 C·m to −6,958 C· m when considering the vertical channel instead of the slanted channel. Although our rebounding-wave model is capable of modeling the rebounding features inside the waveform, the rebounding wave feature for NBE#92 is not obvious due to the strong downward attenuation rate λ_d.

5. Conclusions

In this study, we investigated the propagation effect of slanted NBE sources by using a new rebounding-wave model based on the slanted TL model. The modeling results were first validated against the full-wave FDTD method, and then compared with the observations for both vertical and slanted cases reported in the literature.

The inclination of the NBE channel affects the waveforms and amplitudes of the electrostatic, induction, and radiation components of the electric fields at close distances ($d < 10$ km). However, it only affects the amplitudes of the fields at far distances ($d > 50$ km), where the fields are dominated by the radiation

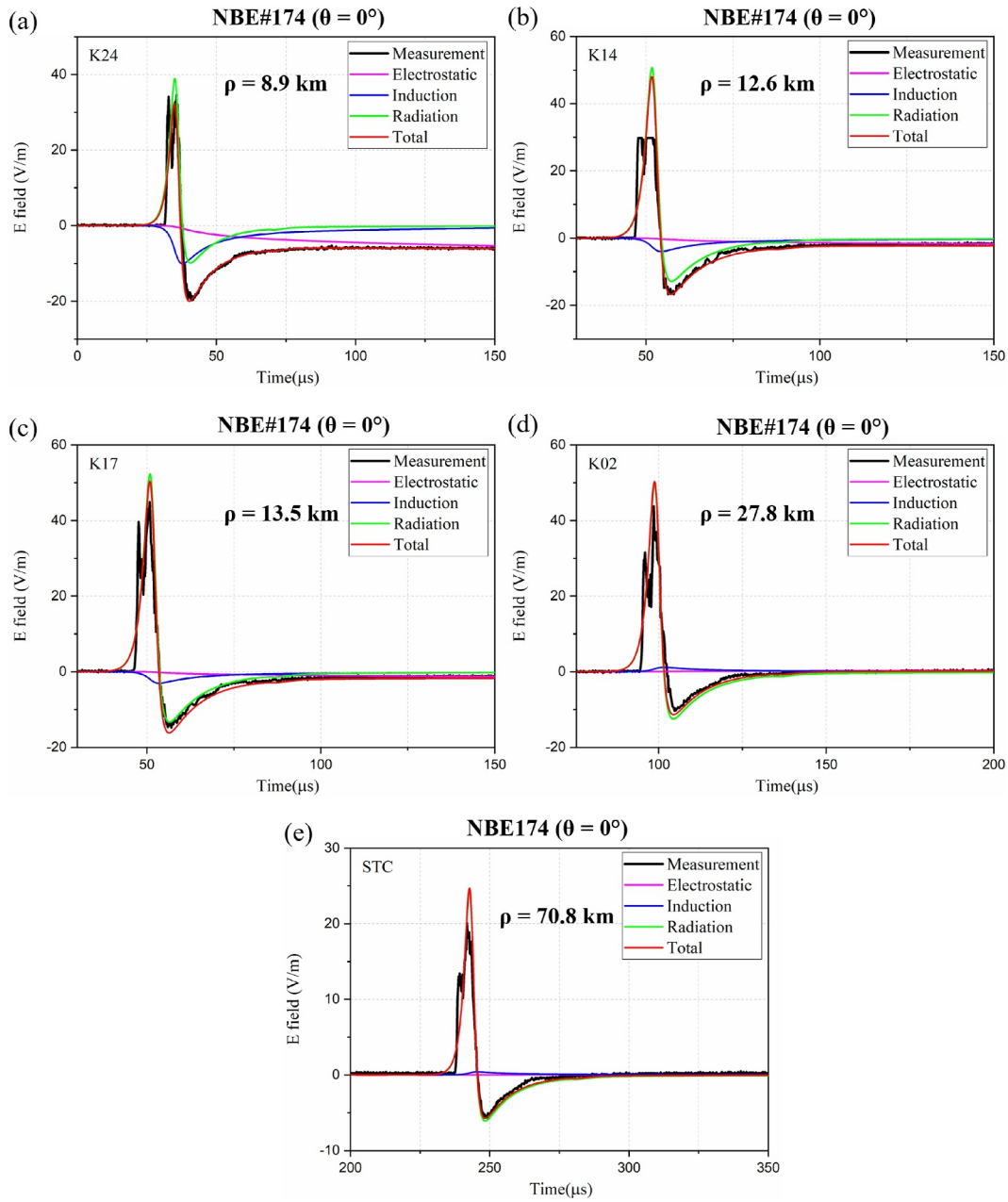

Figure 7. Comparison between the observations from Karunarathne et al. (2016) and simulation results by assuming a vertical channel for NBE#174 at different distances. The electrostatic, induction and radiation components of the total electric fields are also given in the figure.

component. An inclination of less than 30° has a negligible effect (less than 10%) at distances beyond 10 km. In contrast, slant angles greater than 30° can result in field amplitude changes exceeding 30% even at distances of 50 km. For all the slanted cases, the proposed model considering the channel inclination improves the agreement with respect to a purely vertical channel.

Additionally, the effect of the slow electrostatic change following the NBEs was discussed. The results that consider the extra long decay current based on a double-exponential expression match well with the slow electrostatic change in both close and far observations. This suggests that the current of the slow electrostatic

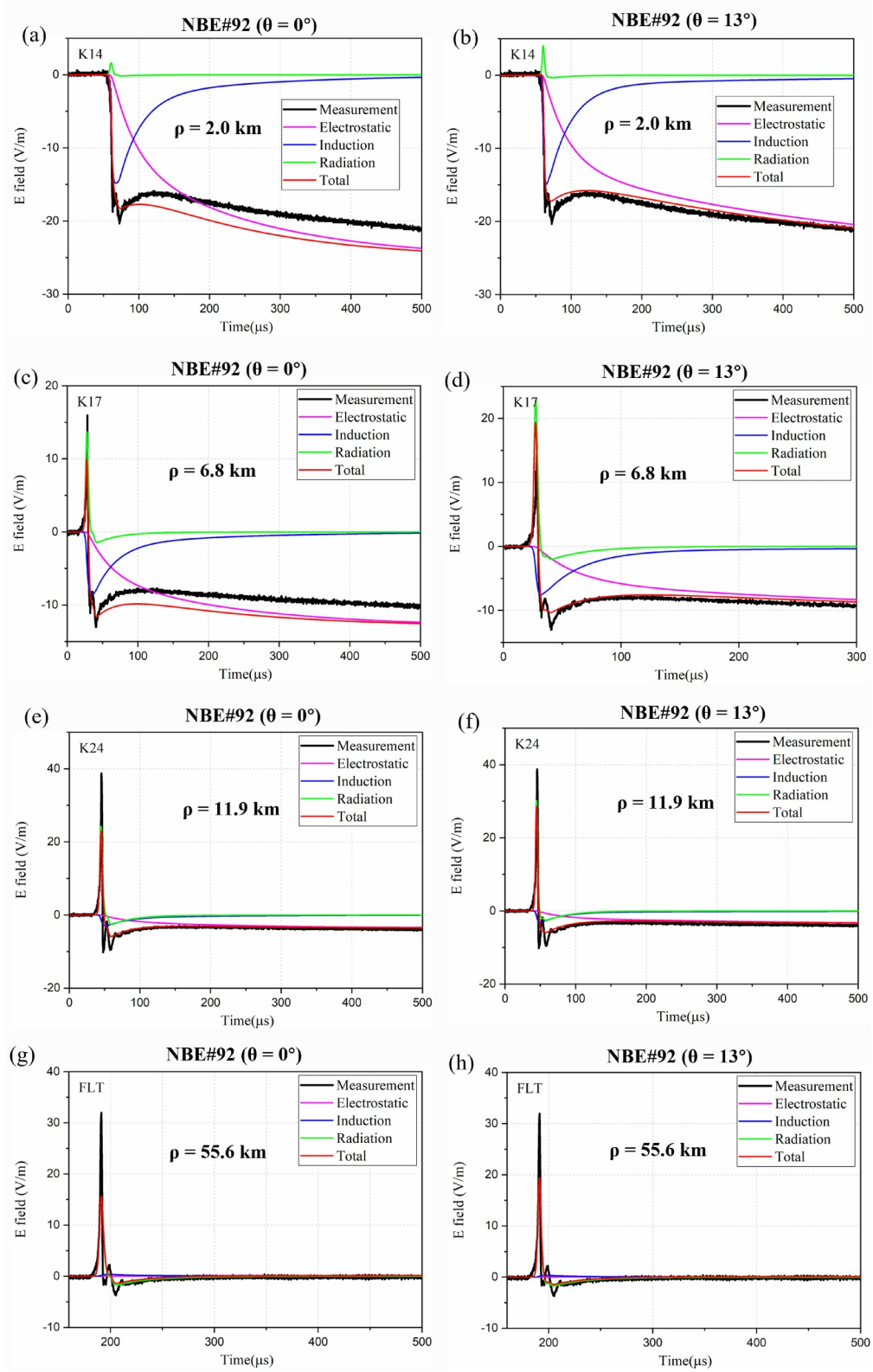

Figure 8. Comparison between the observations from Karunarathne et al. (2016) and simulation results by assuming a vertical channel (a, c, e, g) and a slanted channel (b, d, f, h) for NBE#92 at different distances. The electrostatic, induction and radiation components of the total electric fields are also given in the figure.

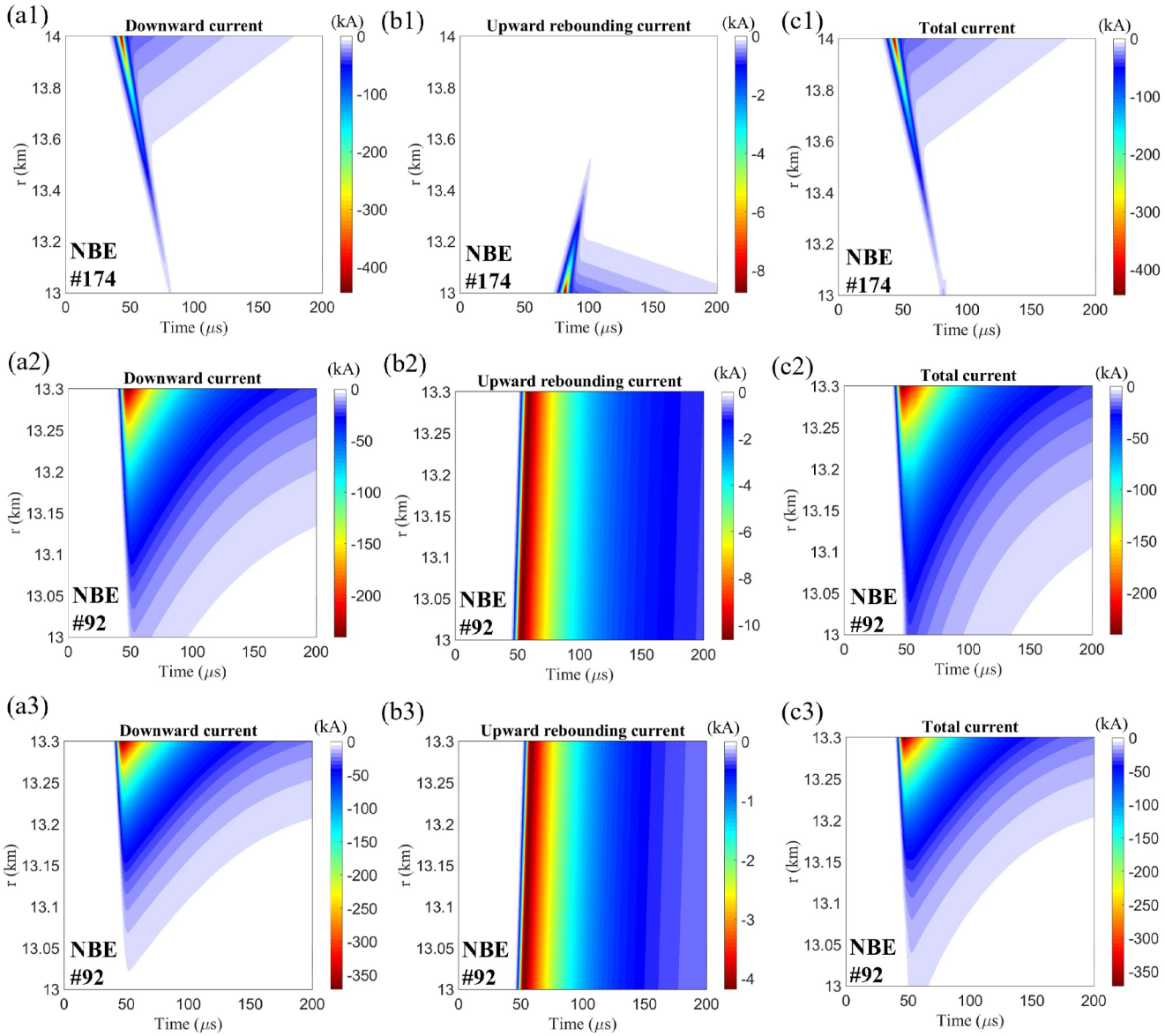

Figure 9. The downward, upward and total current distribution based on the rebounding MTLE model for the vertical NBE#174 (a1, b1, c1) and the vertical NBE#92 (a2, b2, c2) and the slanted NBE#92 (a3, b3, c3) in Karunarathne et al. (2016).

change may actually decrease exponentially, rather than linearly. However, additional observational evidence is required to draw a general conclusion.

Apart from the NBE cases discussed in this study, the suggested equations can be applied to arbitrary observation distances, and, by approximating a curved channel geometry with piecewise linear segments, it can be further extended to any discharge shape.

Data Availability Statement

The data that support the findings of this study are openly available at Li, Luque, Rachidi, et al. (2023).

Acknowledgments
The authors would like to thank Dr. Thomas C. Marshall, Dr. Sumedhe Karunarathne and Dr. Maribeth Stolzenburg at the University of Mississippi for providing data from Karunarathne et al. (2016). This work was supported by the European Research Council (ERC) under the European Union H2020 programme/ERC Grant agreement 681257. Additionally, this work was supported by the Spanish Ministry of Science and Innovation, MINECO, under the project PID2019-109269RB-C43 and FEDER program. D.L. would like to acknowledge the Danish Council for Independent Research for a Danmarks Frie Forskningsfond (DFF) research grant with agreement 1026-00420B and a DFF Sapere Aude Grant (3120-00088B). D.L. and A.L. acknowledge financial support from the State Agency for Research of the Spanish MCIU through the 'Center of Excellence Severo Ochoa' award for the Instituto de Astrofísica de Andalucía (SEV-2017-0709).

References

Abouzeid, S. I., Shabib, G., & Zein El Dein, A. (2015). Analysis of electromagnetic fields generated by inclined lightning channel. *Arabian Journal for Science and Engineering*, *40*(9), 2585–2608. https://doi.org/10.1007/s13369-015-1660-7

Andreotti, A., Petrarca, C., Rakov, V. A., & Verolino, L. (2012). Calculation of voltages induced on overhead conductors by nonvertical lightning channels. *IEEE Transactions on Electromagnetic Compatibility*, *54*(4), 860–870. https://doi.org/10.1109/TEMC.2011.2174995

Attanasio, A., da Silva, C., & Krehbiel, P. (2021). Electrostatic conditions that produce fast breakdown in thunderstorms. *Journal of Geophysical Research: Atmospheres*, *126*(19), e2021JD034829. https://doi.org/10.1029/2021JD034829

Attanasio, A., Krehbiel, P. R., & da Silva, C. L. (2019). Griffiths and Phelps lightning initiation model, revisited. *Journal of Geophysical Research: Atmospheres*, *124*(14), 8076–8094. https://doi.org/10.1029/2019JD030399

Chen, S., Rakov, V. A., Zhu, Y., & Ding, Z. (2024). Clusters of compact intracloud discharges (CIDs) in overshooting convective surges. *Journal of Geophysical Research: Atmospheres*, *129*(8), e2023JD040307. https://doi.org/10.1029/2023JD040307

da Silva, C. L., Merrill, R. A., & Pasko, V. P. (2016). Mathematical constraints on the use of transmission line models to investigate the preliminary breakdown stage of lightning flashes. *Radio Science*, *51*(5), 367–380. https://doi.org/10.1002/2015RS005853

Eack, K. B. (2004). Electrical characteristics of narrow bipolar events. *Geophysical Research Letters*, *31*(20). https://doi.org/10.1029/2004GL021117

Karunarathne, S., Marshall, T. C., Stolzenburg, M., & Karunarathna, N. (2016). Electrostatic field changes and durations of narrow bipolar events. *Journal of Geophysical Research: Atmospheres*, *121*(17), 10161–10174. https://doi.org/10.1002/2016JD024789

Kostinskiy, A. Y., Marshall, T. C., & Stolzenburg, M. (2020). The mechanism of the origin and development of lightning from initiating event to initial breakdown pulses (v.2). *Journal of Geophysical Research: Atmospheres*, *125*(22), e2020JD033191. https://doi.org/10.1029/2020JD033191

Leal, A. F., & Rakov, V. A. (2019). A study of the context in which compact intracloud discharges occur. *Scientific Reports*, *9*(1), 12218. https://doi.org/10.1038/s41598-019-48680-6

Le Vine, D. M. (1980). Sources of the strongest RF radiation from lightning. *Journal of Geophysical Research*, *85*(C7), 4091–4095. https://doi.org/10.1029/JC085iC07p04091

Le Vine, D. M., & Meneghini, R. (1978a). Electromagnetic fields radiated from a lightning return stroke: Application of an exact solution to Maxwell's equations. *Journal of Geophysical Research*, *83*(C5), 2377–2384. https://doi.org/10.1029/JC083iC05p02377

Le Vine, D. M., & Meneghini, R. (1978b). Simulation of radiation from lightning return strokes: The effects of tortuosity. *Radio Science*, *13*(5), 801–809. https://doi.org/10.1029/RS013i005p00801

Li, D., Azadifar, M., Rachidi, F., Rubinstein, M., Diendorfer, G., Sheshyekani, K., et al. (2016). Analysis of lightning electromagnetic field propagation in mountainous terrain and its effects on ToA-based lightning location systems. *Journal of Geophysical Research: Atmospheres*, *121*(2), 895–911. https://doi.org/10.1002/2015JD024234

Li, D., Liu, F., Pérez-Invernón, F. J., Lu, G., Qin, Z., Zhu, B., & Luque, A. (2020). On the accuracy of ray-theory methods to determine the altitudes of intracloud electric discharges and ionospheric reflections: Application to narrow bipolar events. *Journal of Geophysical Research: Atmospheres*, *125*(9), e2019JD032099. https://doi.org/10.1029/2019JD032099

Li, D., Luque, A., Gordillo-Vazquez, F. J., Pérez-Invernón, F. J., Husbjerg, L. S., Neubert, T., et al. (2023a). Different types of corona discharges associated with high-altitude positive narrow bipolar events nearby cloud top. *Journal of Geophysical Research: Atmospheres*, *128*(4), e2022JD037883. https://doi.org/10.1029/2022JD037883

Li, D., Luque, A., Gordillo-Vázquez, F. J., Silva, C. d., Krehbiel, P. R., Rachidi, F., & Rubinstein, M. (2022a). Secondary fast breakdown in narrow bipolar events. *Geophysical Research Letters*, *49*(7), e2021GL097452. https://doi.org/10.1029/2021GL097452

Li, D., Luque, A., Lehtinen, N. G., Gordillo-Vázquez, F. J., Neubert, T., Lu, G., et al. (2022b). Multi-pulse corona discharges in thunderclouds observed in optical and radio bands. *Geophysical Research Letters*, *49*(13), e2022GL098938. https://doi.org/10.1029/2022GL098938

Li, D., Luque, A., Rachidi, F., Rubinstein, M., Neubert, T., Zhu, Y., et al. (2023b). Data for propagation eects of slanted narrow bipolar events: A rebounding-wave model study [Dataset]. *Zenodo*. https://doi.org/10.5281/zenodo.8069595

Li, D., Rubinstein, M., Rachidi, F., Diendorfer, G., Schulz, W., & Lu, G. (2017). Location accuracy evaluation of ToA-based lightning location systems over mountainous terrain. *Journal of Geophysical Research: Atmospheres*, *122*(21), 11760–11775. https://doi.org/10.1002/2017JD027520

Liu, N., & Dwyer, J. R. (2020). Thunderstorm high-frequency radio bursts with weak low-frequency radiation. *Geophysical Research Letters*, *47*(23), e2020GL090325. https://doi.org/10.1029/2020GL090325

Liu, N., Dwyer, J. R., Tilles, J. N., Stanley, M. A., Krehbiel, P. R., Rison, W., et al. (2019). Understanding the radio spectrum of thunderstorm narrow bipolar events. *Journal of Geophysical Research: Atmospheres*, *124*(17–18), 10134–10153. https://doi.org/10.1029/2019JD030439

Lyu, F., Cummer, S. A., Qin, Z., & Chen, M. (2019). Lightning initiation processes imaged with very high frequency broadband interferometry. *Journal of Geophysical Research: Atmospheres*, *124*(6), 2994–3004. https://doi.org/10.1029/2018JD029817

Marshall, R. A., da Silva, C. L., & Pasko, V. P. (2015). Elve doublets and compact intracloud discharges. *Geophysical Research Letters*, *42*(14), 6112–6119. https://doi.org/10.1002/2015GL064862

Marshall, T. C., Bandara, S., Karunarathne, N., Karunarathne, S., Kolmasova, I., Siedlecki, R., & Stolzenburg, M. (2019). A study of lightning flash initiation prior to the first initial breakdown pulse. *Atmospheric Research*, *217*, 10–23. https://doi.org/10.1016/j.atmosres.2018.10.013

Marshall, T. C., Stolzenburg, M., Karunarathna, N., & Karunarathne, S. (2014). Electromagnetic activity before initial breakdown pulses of lightning. *Journal of Geophysical Research: Atmospheres*, *119*(22), 12558–12574. https://doi.org/10.1002/2014JD022155

Nag, A., & Rakov, V. A. (2010). Compact intracloud lightning discharges: 1. Mechanism of electromagnetic radiation and modeling. *Journal of Geophysical Research*, *115*(D20). https://doi.org/10.1029/2010JD014235

Nucci, C. A., & Rachidi, F. (1989). Experimental validation of a modification to the Transmission Line model for LEMP calculation. In *8th symposium and technical exhibition on electromagnetic compatibility, zurich, Switzerland*.

Pervez, Z., Janalizadeh, R., & Pasko, V. P. (2024). Remote sensing of source currents of narrow bipolar events using measured electric fields. *Geophysical Research Letters*, *51*(7), e2023GL107789. https://doi.org/10.1029/2023GL107789

Phelps, C. (1974). Positive streamer system intensification and its possible role in lightning initiation. *Journal of Atmospheric and Terrestrial Physics*, *36*(1), 103–111. https://doi.org/10.1016/0021-9169(74)90070-1

Phelps, C., & Griffiths, R. F. (1976). Dependence of positive corona streamer propagation on air pressure and water vapor content. *Journal of Applied Physics*, *47*(7), 2929–2934. https://doi.org/10.1063/1.323084

Rachidi, F., & Nucci, C. (1990). On the Master, Uman, Lin, Standler and the modified transmission line lightning return stroke current models. *Journal of Geophysical Research*, *95*(D12), 20389–20393. https://doi.org/10.1029/JD095iD12p20389

Rison, W., Krehbiel, P. R., Stock, M. G., Edens, H. E., Shao, X.-M., Thomas, R. J., et al. (2016). Observations of narrow bipolar events reveal how lightning is initiated in thunderstorms. *Nature Communications*, *7*(1), 10721. https://doi.org/10.1038/ncomms10721

Rubinstein, M., & Uman, M. A. (1990). On the radiation field turn-on term associated with traveling current discontinuities in lightning. *Journal of Geophysical Research*, *95*(D4), 3711–3713. https://doi.org/10.1029/JD095iD04p03711

Senay, S., Krehbiel, P. R., da Silva, C. L., Edens, H. E., Bennecke, D., & Stanley, M. A. (2023). Analysis of narrow bipolar events using mode decomposition methods. *Journal of Geophysical Research: Atmospheres*, *128*(21), e2022JD038444. https://doi.org/10.1029/2022JD038444

Shao, X.-M., Fitzgerald, T. J., & Jacobson, A. R. (2005). Reply to comment by rajeev Thottappillil and Vladimir A. Rakov on "radio frequency radiation beam pattern of return strokes: A revisit to theoretical analysis". *Journal of Geophysical Research*, *110*(D24), D24102. https://doi.org/10.1029/2005JD005889

Shao, X.-M., Jacobson, A. R., & Fitzgerald, T. J. (2004). Radio frequency radiation beam pattern of lightning return strokes: A revisit to theoretical analysis. *Journal of Geophysical Research*, *109*(D19), D19108. https://doi.org/10.1029/2004JD004612

Smith, D. A., Heavner, M. J., Jacobson, A. R., Shao, X. M., Massey, R. S., Sheldon, R. J., & Wiens, K. C. (2004). A method for determining intracloud lightning and ionospheric heights from VLF/LF electric field records. *Radio Science*, *39*(1), RS1010. https://doi.org/10.1029/2002RS002790

Smith, D. A., Shao, X. M., Holden, D. N., Rhodes, C. T., Brook, M., Krehbiel, P. R., et al. (1999). A distinct class of isolated intracloud lightning discharges and their associated radio emissions. *Journal of Geophysical Research*, *104*(D4), 4189–4212. https://doi.org/10.1029/1998JD200045

Thottappillil, R., & Rakov, V. A. (2001). On the computation of electric fields from a lightning discharge in time domain. In *2001 IEEE EMC international symposium on electromagnetic compatibility* (Vol. 2, pp. 1030–1035).

Thottappillil, R., & Rakov, V. A. (2005). Comment on "radio frequency radiation beam pattern of lightning return strokes: A revisit to theoretical analysis" by Xuan-Min Shao, Abram R. Jacobson, and T. Joseph Fitzgerald. *Journal of Geophysical Research*, *110*(D24), D24106. https://doi.org/10.1029/2004JD005729

Thottappillil, R., Uman, M. A., & Rakov, V. A. (1998). Treatment of retardation effects in calculating the radiated electromagnetic fields from the lightning discharge. *Journal of Geophysical Research*, *103*(D8), 9003–9013. https://doi.org/10.1029/97JD02941

Tilles, J. N., Liu, N., Stanley, M. A., Krehbiel, P. R., Rison, W., Stock, M. G., et al. (2019). Fast negative breakdown in thunderstorms. *Nature Communications*, *10*(1), 1648. https://doi.org/10.1038/s41467-019-09621-z

Uman, M. A., & McLain, D. K. (1970a). Lightning return stroke current from magnetic and radiation field measurements. *Journal of Geophysical Research (1896-1977)*, *75*(27), 5143–5147. https://doi.org/10.1029/JC075i027p05143

Uman, M. A., & McLain, D. K. (1970b). Radiation field and current of the lightning stepped leader. *Journal of Geophysical Research (1896-1977)*, *75*(6), 1058–1066. https://doi.org/10.1029/JC075i006p01058

Uman, M. A., McLain, D. K., & Krider, E. P. (1975). The electromagnetic radiation from a finite antenna. *American Journal of Physics*, *43*(1), 33–38. https://doi.org/10.1119/1.10027

Watson, S. S., & Marshall, T. C. (2007). Current propagation model for a narrow bipolar pulse. *Geophysical Research Letters*, *34*(4), L04816. https://doi.org/10.1029/2006GL027426